

Geometric and Electromagnetic Aspects of Fusion Pore Making

D. Apushkinskaya, E. Apushkinsky, B. Booss-Bavnbek, and M. Koch

1	Introduction	2
1.1	Electromagnetic Free Boundary Route to Fusion Pore Making	2
1.2	Plan of the Chapter	3
2	Synopsis of Established Facts	3
2.1	Membrane Fusion and the Fusion Pore Challenge	3
2.2	Competing Mathematical Approaches to Space-Time Processes	5
2.3	Oscillatory Intracellular Release and Binding of Ca^{2+} Ions	7
2.4	The Magnetic Character of the Induced Field Wave	10
2.5	Dimple Formation Prior to the Fusion Event	13
2.6	The Flickering of Regulated Exocytosis	15
3	The Model	16
3.1	The Force Balance Equation	16
3.2	The 1D-Case	16
3.3	The 2D-Case	18
3.4	Further Approximations	20
3.5	Lorentz Force	20
4	Apposite Results on Parabolic Obstacle Problems	23
4.1	Review of Free Boundary Problems	23
4.2	Qualitative Properties of Solutions	24
4.3	Classification of Blow-up Limits in \mathbb{R}^{n+1}	25
4.4	Classification of the Free Boundary Points	25
5	Conclusions	26
5.1	The Findings	27

Darya Apushkinskaya

Fachbereich Mathematik, Universität Saarbrücken, Postfach 151150, D-66041 Saarbrücken, Germany, e-mail: darya@math.uni-sb.de

Evgeny Apushkinsky

Experimental Physics Department, St. Petersburg State Polytechnical University, St. Petersburg, Russia, e-mail: apushkinsky@hotmail.com

Bernhelm Booss-Bavnbek

Roskilde University, IMFUFA, Dept. of Science, Systems and Modelling, DK-4000 Roskilde, Denmark, e-mail: booss@ruc.dk

Martin Koch

Feldkraft Ltd., Højbovej 11, DK-2500 Copenhagen, Denmark, e-mail: mko@mail.tele.dk

5.2	Suggested Experiments and Measurements	27
	References	28

Abstract For regulated exocytosis, we model the morphology and dynamics of the making of the fusion pore or porosome as a cup-shaped lipoprotein structure (a *dimple* or *pit*) on the cytosol side of the plasma membrane. We describe the forming of the dimple by a free boundary problem. We discuss the various forces acting and analyze the magnetic character of the wandering electromagnetic field wave produced by intracellular spatially distributed pulsating (and well observed) release and binding of Ca^{2+} ions anteceding the bilayer membrane vesicle fusion of exocytosis. Our approach explains the energy efficiency of the observed dimple forming prior to hemifusion and fusion pore and the observed flickering in secretion. It provides a frame to relate characteristic time length of exocytosis to the frequency, amplitude and direction of propagation of the underlying electromagnetic field wave.

Key words: Calcium oscillations; free boundary problems; dimple formation; fusion pore; Lorentz force; Maxwell equations; pancreatic beta-cell; plasma membrane; regulated exocytosis.

1 Introduction

This chapter adds a few electromagnetic facts and mathematical theorems to the toolbox approaching the process of bilayer membrane vesicle fusion. We address the related geometric and dynamic aspects of the endocytotic-exocytotic cycle which is at the core of various discharge (e.g., secretion) and ingestion (e.g., drug intake) processes in animal cells.

1.1 Electromagnetic Free Boundary Route to Fusion Pore Making

For regulated exocytosis, we model the morphology and dynamics of the making of the fusion pore or porosome as a cup-shaped lipoprotein structure (a *dimple* or *pit*) on the cytosol side of the plasma membrane. One ingredient to our model is a free boundary problem for the dimple under the action of electromagnetic forces, in particular the Lorentz force acting on charged phospholipid molecules of the cell's plasma membrane with decreasing capacitive reactances while forming the dimple. The force comes from a wandering electromagnetic field produced by intracellular spatially distributed pulsating (and well observed) release and binding of Ca^{2+} ions.

Our approach is based on variational principles and emphasizes regularity and singularity under the deformation process of the membranes. It explains the energy efficiency of the observed dimple forming prior to hemifusion and fusion pore and the observed flickering in secretion. It provides a frame to relate characteristic time

length of exocytosis (ranging between milliseconds in nerve cells and seconds in β -cells) to the frequency, amplitude and direction of propagation of the underlying electromagnetic field wave.

We shall not address all the *machines* (both protein machines and lipid assemblies) working together in making the structure and the composition of the fusion pore. Admittedly, conclusive evidence is still lacking of the critical character of the here described electromagnetic field wave for the well-functioning of the regulated exocytosis in healthy cells and the lack of secretion robustness in stressed cells. In germ, however, the present electromagnetic free boundary model gives various hints to future calculations, estimates, and in *vivo*, in *vitro* and in *silico* (i.e., numerical simulation) experiments.

1.2 Plan of the Chapter

In Sect. 2 we summarize several mathematical, electrodynamical and cell physiological facts which seemingly have been overlooked or discarded in the literature, but may in our perception add essential ingredients to a comprehensive understanding of the short very first phase of regulated exocytosis. In Sect. 3 we describe our model and the corresponding differential equations, force balances and cost functionals. In Sect. 4 we discuss regularity and singularity results. In Sect. 5 we present our preliminary conclusion; some hints regarding the question of what controls the speed of the process; and a review of experimental tasks and capabilities to test our hypotheses.

2 Synopsis of Established Facts

We describe the challenge of making the fusion pore; distinguish different mathematical modelling approaches; and elaborate electromagnetic and geometric phenomena of the very first phase of regulated exocytosis, namely Ca^{2+} oscillations, the corresponding slow and low frequent electromagnetic field wave, and the forming of a dimple in the plasma membrane prior to the bilayer membrane vesicle fusion.

2.1 Membrane Fusion and the Fusion Pore Challenge

Membrane fusion is fundamental to transport phenomena in animal cells mediated by vesicular traffic. That happens when cells ingest fluid and macromolecules by *endocytosis*, in which, in the suggestive words of a renown textbook “localized regions of the plasma membrane invaginate and pinch off to form endocytic vesicles”

(Alberts et al., [1]). The opposite process, when animal cells discharge material, after collecting it in vesicles, is called *exocytosis* and is our subject.

It happens by pulling and docking the vesicle on the cell membrane through activity of transmembrane proteins, followed by membrane-vesicle hemi-fusion and the making of a fusion pore in the membrane through which the material can be ejected or poured out, see Fig. 1. As a rule, the two processes seem to be bal-

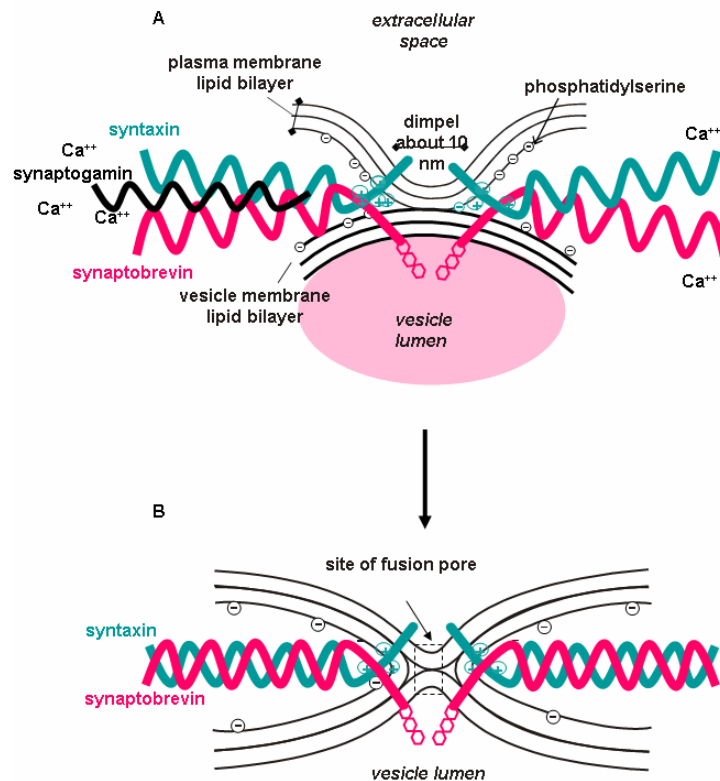


Fig. 1 Schematic view of the bilayer membrane fusion event, from Koch et al. [2] (after Lentz [3]), reproduced with permission of World Scientific Publishers and the authors. Shown are the basic molecular structures involved in the process of fusion pore making and membrane fusion. Note the lipid bilayers of the plasma membrane and the vesicle membrane, with the negative charges representing the charged heads of phosphatidyl serine. For clarity, only the transmembrane proteins syntaxin and synaptobrevin with the three aromatic amino acids on the luminal side of the vesicle membrane are depicted. Also included is synaptogamin, which binds Ca²⁺ and is associated to both syntaxin and synaptobrevin.

anced, the one cutting membrane pieces out of the cell membrane, the other inserting pieces. In both processes, the remarkable is opening of the cell *without* pinching a hole.

Typical examples of endocytosis are the intake of nutrition, signal molecules, viruses or drugs; typical examples of exocytosis are secretory processes like waste removal, neurotransmitter secretion of nerve cells or insulin secretion of β -cells of the Langerhans islands in the pancreas. It seems that a better understanding of these two processes could, e.g., support the early diagnosis of metabolic diseases, like diabetes mellitus type 2 (exocytic dysfunction, see Rorsman and Renström [4, 5]) or a more efficient delivery of insulin analogues (inducing endocytosis, see de Meyts [6]).

Recent advances in observational and manipulative nano techniques and in mesoscopic coarse-grained computer simulation have provided substantial progress in visualizing, understanding - and possibly - influencing the bilayer membrane vesicle fusion (for a recent systematic review we refer to Shillcock and Lipowski [7]). With present technology, however, the observational findings are hampered by a kind of Heisenberg Inequality: geometric shape *and* the parameters of change can not be measured to the wanted degree of precision, *simultaneously*. So [7], p. S1196 deplors that “the molecular rearrangements that take place during the final stage of the fusion process, where the two initially distinct membranes join and produce a fusion pore, cannot yet be resolved by these experimental techniques” while “understanding how the stability of lipid membranes is overcome by the cellular protein machinery when required is a major topic of research” (l.c.). This is the challenge which we wish to address by summarizing various mathematical, electrodynamic and empirical facts. Seemingly, these facts have been overlooked or discarded in the literature. We shall show, however, to what extent these facts yield, in our perception essential, ingredients to a comprehensive understanding of this short very first phase of regulated exocytosis.

2.2 Competing Mathematical Approaches to Space-Time Processes

We shall distinguish three different mathematical-numerical approaches to modelling spatial-temporal process of regulated exocytosis: highly aggregated compartment models, spatially distributed dynamical systems, and space-time integrating partial differential equations, where our focus will be. Clearly, all three approaches admit extensions from rigid, stiff and hence fragile deterministic to more robust stochastic modelling. Here, however, we shall not discuss such extensions.

A first class of mathematical exocytosis models are *Compartment Models*, first introduced by Grodsky [8] in 1972, assuming that there are two compartments (pools) of insulin granules, docked granules ready for secretion and reserve granules. By assuming suitable flow rates for outflow from the docked pool and resupply from the reserve pool to the docked pool, the established biphasic secretion process of healthy β -cells could be modelled *qualitatively* correct. By extending the number of pools from two to an array of six and properly calibrating all flow rates, Chen, Wang and Sherman in [9] obtained a striking *quantitative* coincidence with the observed biphasic process, see also Larsen and Pedersen [10] in this volume. The nice

thing of such compartment models is that they invite the experimentalists (both in imaging and in proteomics) to verify the distinction of all the hypothetical compartments in cell reality and to assign biophysical values to the until now only tuned flow rates. A self-imposed limitation is the low resolution of the aggregated compartments which does not allow to investigate the local geometry and the energy balance of the secretion process.

On the opposite length and time scale, we have a second class of mathematical models, namely the impressive numerical analysis of the bilayer membrane vesicle fusion by *Molecular Dynamics* (MD), *Monte Carlo simulations* (MC) and *Dissipative Particle Dynamics* (DPD) on nanometer distances and fractions of nanoseconds, based on gravitational and electric forces between the particles, see the afore cited [7] and Shillcock, [12] in this volume. Unfortunately, these computer simulations are also seriously hampered, namely by limitations of present hardware and software when one is addressing mesoscopic behavior, i.e., changes across many scales of the molecular characteristics - in spite of the impressive results when applying these methods to phenomena on the nano scale, like modelling the island dynamics of film crystallization in epitaxial growth driven by molecular beam epitaxy, see, e.g., Cafilisch and Li [13]. These limitations in present computer capacity require MD, MC and DPD simulations to make *a priori* assumptions about the *pathway* of the fusion process, e.g., spherical symmetry of the vesicles and planarity and circularity of the fusion pores - besides the often deplored “enormous gap between the sophistication of the models and the success of the numerical approaches used in practice and, on the other hand, the state of the art of their rigorous understanding” (Le Bris [14] in his 2006 report to the International Congress of Mathematicians). To keep these models transparent, a self-imposed limitation is their focus on the local neighbourhood of the fusion event, neglecting long-distance phenomena like electromagnetic waves across the cell.

Whereas compartment models respectively MD and DPD are built upon small respectively huge systems of ordinary differential equations with each unknown specifying temporal changes in one given pool or spatial box, we advocate a third class of mathematical models, namely modelling the dynamics and the geometry by *partial differential equations*. Consequently, we shall try to model the relevant processes by one or two spatial-temporal equations based on First Principles, instead of the few aggregated purely temporal pool equations in compartment modelling or the three millions of purely temporal equations for spatially distributed boxes in [7], p. 1197 (which still is a very poor particle number for a $100\text{ nm} \times 100\text{ nm} \times 42\text{ nm}$ simulation box).

Moreover, the simplicity of our fundamental equations admits a transparent incorporation of long-distance phenomena. In such a way, our approach takes its point of departure not alone in the rather well studied *elastic* and *electric* properties and potentials of and across the plasma membrane and the *viscosity* of the cytosol, but in non-stationary, dynamic *electromagnetic* properties. To us, the basic electromagnetic character of the fusion process becomes evident in

- the observed electromagnetic (wandering) field waves, see Sect. 2.3,

- the closure of the corresponding magnetic wave over the plasma membrane, see Sect. 2.4,
- the observed forming of a narrow dimple, solely to be understood like a capacitor, see Sect. 2.5, and
- the observed flickering of the secretion process corresponding to the natural variability of the (wandering) field wave generation, see Sect. 2.6.

The goal of our approach is

1. to develop a simple free boundary model for the dimple forming process, see Sect. 3,
2. to focus on regularity and possible singularity of the free boundary, see Sect. 4,
3. to provide a reliable framework for estimating (and, hopefully, influencing) the parameters which control the speed of the process, see Sect. 5.1,
4. and to formulate a bundle of model-based observation plans to verify or falsify our assumptions, see Sect. 5.2.

Our approach is inspired by recent work of A. Friedman and collaborators about tumor growth, see [15]–[18]; by a theoretical analysis of adhering lipid vesicles with free edges, see [19] by Ni, Shi, and Yin; by the electrodynamic challenge to understand the observed Ca^{2+} oscillations, rightly perceived as being “contradictory and often do not support the existing (electrostatic) models” (Fridlyand and Philipson [20]) and by the mathematical challenge to understand the (in elastic terms counter-intuitive) dimple formation so well described in the literature, see, e.g., Monck and Fernandez [22], Rosenheck [23], Lentz et al. [3], Koch et al. [2].

2.3 Oscillatory Intracellular Release and Binding of Ca^{2+} Ions

By fluorescence microscopy, empirical evidence has been provided about pulsating Ca^{2+} activity at extreme low frequency $f \sim 0.1 \text{ Hz} \ll 3 \text{ Hz}$ (for comparison, the house low frequency grid is of 50 Hz, i.e., spikes in intervals of 20 msec), prior to the fusion event, see Kraus, Wolf and Wolf, [24] and Bernhard Wolf’s homepage [25] with informative video animations of calcium oscillations, and the comprehensive review and analysis by Salazar, Politi and Höfer, [26].¹

The following can be seen in many cell types: after polluting the cell with a macromolecule, changes in the cytosolic calcium concentration $[\text{Ca}^{2+}]_c$ occur as

¹ Our model cell is a pancreatic β -cell where a single release is slow and may take seconds. Correspondingly, we expect a low Ca^{2+} oscillation rate in intervals in the range of seconds yielding extreme low frequency of the observed 0.1 Hz. For nerve cells the reaction time, and so the release time, is in the range of msec, possibly less than 100 μsec , see Jahn, Lang, and Südhoff [27]. Correspondingly, we expect a high Ca^{2+} firing rate in intervals of, e.g., 10 msec yielding a frequency of 100 Hz with associated high energy losses. So, our electromagnetic free boundary route to vesicle fusion can not function in nerve cells unless the neurotransmitter vesicles are kept waiting very close to the plasma membrane. Here our finding coincides with the well-known deviating high energy consumption of nerve cells. We shall elaborate this aspect in Sect. 5 below.

repetitive spikes that increase their frequency with the strength of the stimulus (see also Berridge, Bootman, and Roderick [28] and Gaspers and Thomas [29]). It is well known that an increase in $[Ca^{2+}]_c$, ultimately, regulates a plethora of cellular processes mediated by Ca^{2+} -dependent enzymes that, in turn, modify downstream targets commonly by phosphorylation.

Investigating Ca^{2+} decoding in an analytically tractable model, Höfer and collaborators address the question “Under which conditions are Ca^{2+} oscillations more potent than a constant signal in activating a target protein?” in [26, p. 1204] in complex biochemical terms of binding and release rates of Ca^{2+} ions. We wish to supplement these investigations by elaborating the electromagnetic character of the Ca^{2+} oscillations. Roughly speaking, the following is happening in electromagnetic terms: Based on information obtained from the cell neighborhood and from inside the cell, possibly mediated by the nucleus, an array of Ca^{2+} storages (e.g., the mitochondria and the smooth endoplasmic reticulum - SER, see also [20, Section 5]) is activated. These organelles sequester Ca^{2+} when the cytosolic concentration $[Ca^{2+}]_c$ is high and release it when $[Ca^{2+}]_c$ is low, relative to cell tasks to perform and cell safety to preserve. In such a way, the organelles build an alternating electric current density (also “displacement vector field”) \mathbf{D} of low frequency by superposition of spatially distributed, temporally coordinated and directed Ca^{2+} activity. As usual in electrodynamics, we shall speak of two different electric fields, \mathbf{D} and \mathbf{E} . This second electric field \mathbf{E} is given by the relation $\mathbf{D} = \epsilon\mathbf{E}$, where $\epsilon = \epsilon_0\epsilon_r$ denotes the dielectric constant. Note that our writing of all electromagnetic units and equations follows Jackson [21] in the units V, A, sec, and m with, e.g., $kg=VAsec^3/m^2$ of the System International - SI, which is predominant in engineering literature.

A physical model of generating electromagnetic field waves by spatially and temporally distributed excitation was built by Koch and Stetter, see <http://www.feldkraft.de/>. It is called *Dynamical Marker* and consists of a couple of coil arrays, electronically regulated for direction-, frequency- and amplitude-controlled generation of a field wave. The instrument has been applied in various cell physiological experiments for slow and efficient transport of beads into cells across the plasma membrane.

There are a couple of related questions which will require separate investigation (see also below Sect. 5.2):

1. How strong is the evidence that the Ca^{2+} oscillations, contrary to the membrane process of Ca^{2+} bursts, originate from an array of Ca^{2+} depots (SER and mitochondria), organized in directed lines?
2. How does the cell select the Ca^{2+} storages to participate in the generation of the alternating current?
3. How is the sequential release and binding of the Ca^{2+} ions of the different storages controlled, i.e., how is the correct spatial and temporal coordination of release and binding obtained?
4. What role plays the observed branching of mitochondria in active β -cells, contrary to the dipol shape of mitochondria in tired β -cells?
5. Can the magnetic character of the field wave, which is produced by low frequent Ca^{2+} oscillations, be influenced via an external field with similar character?

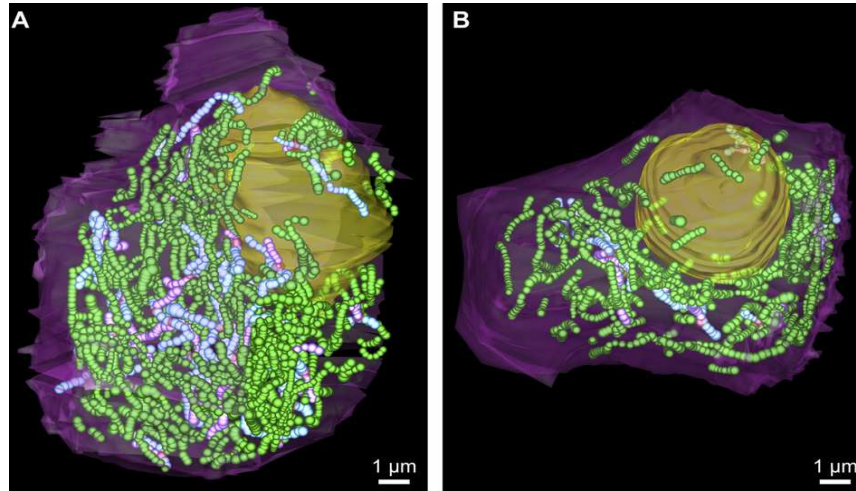


Fig. 2 Functional heterogeneity: left, a multitude of *branched* mitochondria in a vigorously responding β -cell; right, relatively more non-branched *dipole* mitochondria in a less active cell at a comparable locus; branch points are highlighted with red spheres. The panels are from Noske et al., [30] and reproduced with permission of Elsevier. High resolution originals were supplied by courtesy of B. Marsh, University of Queensland, Brisbane, Australia.

To Questions 1 and 2, it may be mandatory to distinguish between two different types of Ca^{2+} burst: the Ca^{2+} *oscillations* addressed here are prior to the secretion and are, presumably, generated by arrays of activated calcium depots distributed through the full length of the cell. On the contrary, the Ca^{2+} *influx* through the ion channels of the plasma membrane during regulated exocytosis is mainly effective *close* to the plasma membrane where it increases the concentration $[\text{Ca}^{2+}]_c$ and changes the electric potential across the plasma membrane. It is worth mentioning that the array character is evident from the observed oscillations in the form of *directed, oriented waves*.

To Question 3, we imagine that the coordination of the activity of the participating Ca^{2+} storages is not controlled externally, e.g., by the nucleus, but happens spontaneously by selforganization: we notice that the storages of molecular calcium sense and respond to stimuli by periodic release and binding of Ca^{2+} ions and suppose that the sequential coordination between spatially distributed loci of release and binding minimizes the energy consumption for maintaining the activity and for establishing a suitable average concentration $[\text{Ca}^{2+}]_c$.

To Question 4, we recall from Noske et al [30] a remarkable discovery. The authors imaged and reconstructed two β -cells from the same glucose-stimulated mouse islet by single axis, serial section electron microscope tomography (ET) at magnifications of $4700\times$ and $3900\times$, respectively, that resulted in whole cell tomograms with a final resolution of 15-20 nm. In addition, they developed several new methods for the abbreviated segmentation of both cells' full complement of

mitochondria (i.e., the most prominent Ca storages) and insulin secretory granules for comparative analysis. 3D reconstruction by ET of each of the two β -cells (designated 'ribbon01' and 'ribbon02') indicated that ribbon01 responded more vigorously to glucose-stimulation than ribbon02 and contained about twice as many branched mitochondria (26 out of a total number of 249 mitochondria) as ribbon02 (with 10 branched mitochondria out of a total of 168 mitochondria). See also the recent Marsh and Noske [31] in this volume.

Now, from our electromagnetic point of view, the advantage of branched mitochondria is clear for the generating of a field wave. (i.e., the pulsating Ca^{2+} oscillations through the whole length of the cell): a single (non rotating) dipole can not generate or initiate a (directed, oriented) field wave. That *requires* a branched structure with spatially and temporally shifted serial activity, as demonstrated also in the design of the mentioned simple field generator by Koch and Stetter. Of course, nature's regulation of the ion firing may be much more sophisticated than the crude engineering design of the "Dynamic Marker". After all, the eukaryotic cells had many more years to test and optimize different designs in evolution.

To Question 5, we refer to an experimental setting described below in Sect. 5.2.

2.4 The Magnetic Character of the Induced Field Wave

Perhaps one of the most delicate of Maxwell's equations is his modification of Ampère's Law by adding the displacement current density $\frac{\partial \mathbf{D}}{\partial t}$ on the right, i.e., the electric side:

$$\text{curl } \mathbf{H} = \mathbf{J} + \frac{\partial \mathbf{D}}{\partial t}, \text{ respectively } \int_C \mathbf{H} ds = \int_A \left(\mathbf{J} + \frac{\partial \mathbf{D}}{\partial t} \right) d\mathbf{A}. \quad (1)$$

Here \mathbf{H} denotes the oriented, electrically generated magnetic field, $\mathbf{B} = \mu_0 \mu_r \mathbf{H}$ the corresponding magnetic flux density (also "magnetic induction") of frequency f and amplitude $\hat{\mathbf{B}}$, and \mathbf{J} the current density vector for a conductor crossing an area A which is bounded by a contour C . Moreover μ_0 and μ_r denote the absolute and relative magnetic permeability.

Equation (1) is our basic equation regarding the magnetic character of the observed Ca^{2+} oscillations. Note that our field wave can not be compared with an electromagnetic high frequency wave in radio transmission. Its propagation velocity is comparable to sound waves in water and far below light velocity. Moreover, because of the low frequency of our oscillations, the displacement current density $\frac{\partial \mathbf{D}}{\partial t}$ is relatively small. That indicates that the magnetic character dominates the electric character of the field wave.

While a wave with dominant electric character has large losses in cytosol (which is comparable to salty water in its electric conductivity), the magnetic character makes the propagation almost free of losses. To sum up, by the described intracellular Ca^{2+} oscillations a field is generated with only marginal losses because the transmission is almost independent of the material constant ϵ_r . As a result, the moving

Ca^{2+} ions from the intracellular distributed storages are in fact an AC current, generating a nearly loss-free moving (wandering) magnetic *field wave* which transfers energy to a selected transmembrane subregion of the cytosol between the plasma membrane and the vesicle. As we shall explain, this energy and the corresponding forces act on the free lipid ions in the plasma membrane and pull the plasma membrane towards the vesicle. See also [32] for a video animation of a macroscopic field wave.

Our biophysical approach is classical, hence we assume that there are no sources for magnetism, no magnetic monopoles, at least not present in our β -cell. Consequently, we obtain from Maxwell's equations $\text{div} \mathbf{B} = 0$, i.e., the magnetic field wave induced by the alternating current is *closed* in the sense of vector analysis and, consequently, the path of the field wave is closed.

Of course, it must be investigated in detail *how* the magnetic wave is closed. Fluorescence microscopy gives the impression that the observed Ca^{2+} oscillations are collective phenomena of cell ensembles: the oscillations propagate through the ensemble like chained waves. We, however, assume that all magnetic waves are separated from each other and are closed over the single plasma membranes. One reason is that the plasma membrane is perforated by a multitude of ion channels created and maintained by the presence of enzymes like various kinases and phospholipases. Most enzymes contain Fe atoms, see Jensen [33, pp. 134f] and the review on iron biominerals [34]. Consequently, the magnetic field wave will search for a circuit through the plasma membrane.

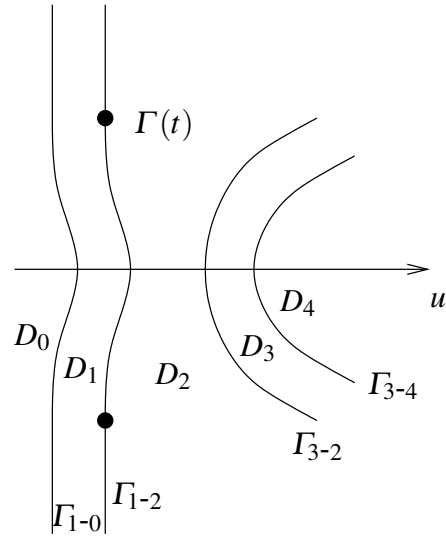
While we have put the determination of the Fe content of the plasma membrane on our experimental agenda below in Sect. 5.2, we better mention that the magnetic permeability μ_r can not be measured directly. However, there have been developed methods to determine the magnetic permeability $\mu_r \sim 1.0000007$ of haemoglobin of deoxidized venous blood non invasively in a precise way. Similar methods will be applicable for investigating the plasma membrane of life cells. Roughly speaking, the indirect methods work by comparative measurements after inflicting a magnetic pollution on a harmonic oscillator.

Now it is not difficult to understand the making of the fusion pore and the dimple formation (see the following Sect. 2.5 for the empirical evidence) in qualitative terms. Let us fix the notation. By electron microscopy, we can distinguish the following clearly separated regions:

- D_0 Amorphous outside cell neighbourhood
- D_1 Plasma membrane with boundary $\partial D_1 = \Gamma_{1-0} \cup \Gamma_{1-2}$
- D_2 Cytosol
- D_3 Vesicle membrane with boundary $\partial D_3 = \Gamma_{3-2} \cup \Gamma_{3-4}$
- D_4 Vesicle lumen
- M_j Activated molecular Ca storage organelles, $j = 1, \dots, n$ (not depicted)
- N Cell nucleus (not depicted).

Note that the region D_1 (the plasma membrane) consists of a phospholipid bilayer. It has a surface Γ_{1-0} as its outside boundary (towards the amorphous outside cell neighborhood D_0) and a surface Γ_{1-2} as its inside boundary (towards region

Fig. 3 Plasma membrane section with cone like dimple (left) under transversal displacement u and spherical vesicle (right) before docking. For a regular cone shaped dimple, the two bold dots mark the circular base line $\Gamma(t) = \partial\{(x,y,z) \mid u(x,y,z,t) \geq 0\}$ of the dimple at time t . In space-time, the union $\{\Gamma(t) \times \{t\}\}_{t \geq 0}$ of the t -components $\Gamma(t)$ form the free boundary Γ , see below Sect. 4.1 before Eq. (16) and Sect. 4.4



D_2 of the watery cytosol within the cell close to the plasma membrane). Moreover, we have the region D_3 consisting of the vesicle membrane (same material like D_1) and the region D_4 , the interior of the vesicle, containing the material to be released through the plasma membrane. Moreover, there is a multitude of activatable Ca^{2+} storage organelles $\{M_j\}$ spread through the interior of the cell. Finally, we have the cell nucleus N , see the abstraction of Fig. 1 in Fig. 3. Typical approximate diameters are $10 \mu\text{m}$ for most animal cells; $5 \mu\text{m}$ for the nucleus; 100 nm for the vesicles; and 8 nm for plasma and vesicle membrane.

In the preparation of the fusion event and the making of the fusion pore, there are apparently only two active regions, in addition to the cell nucleus and the mitochondria and other Ca storages, namely the plasma membrane D_1 and the cytosol D_2 . The plasma membrane D_1 forms a conical inside oriented *dimple* (pit) towards the vesicle of around 10 nm base diameter and $10\text{-}20 \text{ nm}$ height. For the true lipid bilayer membrane-vesicle fusion event, following the making of the dimple, so-called transmembrane proteins become active in the cytosol region D_2 between plasma membrane dimple and the vesicle and pull and dock the vesicle membrane D_3 to the plasma membrane D_1 over a distance of up to 100 nm (see also Fig. 1).

When the deformation of the plasma membrane is sufficiently sharp it ends in a branch point, i.e., a singularity of Γ_{1-2} , called hemifusion. Then it comes to a break-through (called fusion pore), and the content of the vesicle begins to diffuse from the vesicle compartment D_4 into the outside region D_0 . It appears that this process sometimes is interrupted (so called *flickering*, see below), i.e., the fusion pore is hardly maintained by elastic forces alone but needs probably the presence of an electromagnetic field and is interrupted when this magnetic field is interrupted.

What is controlling the well-functioning of the fusion event?

Working hypothesis 1: The regions

$$D_0 (X_C = 0), \quad D_1 (\text{variable } X_C(x,t)) \quad \text{and} \quad D_2 (X_C = 0) \quad (2)$$

are distinguished by their *capacitive reactance* $X_C := 1/(\omega C)$ where $\omega = 2\pi f$ with constant f and C denotes the capacitance. Note that forming the dimple produces an increase of the dielectricum (between the “plates”) and so implies increasing C and decreasing X_C until X_C vanishes in the fusion pore.

Working hypothesis 2: The vesicle is densely packed with material and so not subjected to deformations easily.

Working hypothesis 3: We envisage the following feedback mechanism for forming the dimple and preparing the fusion event.

1. The Ca^{2+} ions from locally distributed intracellular Ca-molecule storages start low frequent oscillations, as described in [24], which are superposed in a controlled way, and a dynamic field wave is produced pointing to a specific region $D_{2,\text{crit}}$ selected for most suitable membrane-vesicle fusion. To begin with, the magnetic flux density vector \mathbf{B} (“magnetic induction”) is low because the magnetic wave doesn’t enter easily the plasma membrane D_1 to close itself in a circuit because of the originally high X_C in D_1 .
2. The form change decreases X_C close to the emerging dimple. That permits the magnetic wandering wave to enter D_1 more easily and so increases its current density (the sharpness of its pointing) and its amplitude \hat{B} . And so on.

2.5 Dimple Formation Prior to the Fusion Event

In the introduction to this chapter we defined the fusion pore as the molecular structure that transiently connects the lumens of two membrane compartments during their fusion. We emphasized that making the fusion pore plays a key role in all intracellular trafficking and endocytotic and exocytotic pathways in all eukaryotic cells, including the regulated exocytosis in endocrine, exocrine and neuronal cells like our β -cell. However, from Monck and Fernandez [22, 1992] to Shillcock and Lipowski [7, 2006], researchers agreed that *despite its importance, the nature of the fusion pore is unknown* ([22, p. 1395]).

In a remarkable series of micrographs, based on rapid freezing techniques for electron microscopy, the reknown expert on mammal egg cells, Douglas Chandler of Arizona State University and collaborators captured the formation of the fusion pore in mast cells already some 30 years ago, [35, 36, 37]. They demonstrated that the pores are made of a curved bilayer which spans the granule and plasma membrane. The micrographs also gave a hint of the events preceding the making of the fusion pore: namely the formation of a dimple that approaches the granule membrane after stimulation, see Figures 4 and 5.

Since then, the dimple formation has been observed in many different cell types immediately upon stimulation before the fusion event, see, e.g., Jena and collaborators [38]. Using atomic force microscopy (AFM) they demonstrated the presence



Fig. 4 Cross section through plasma membrane with dimple and, at the bottom a glimpse of the granule. Electron micrograph supplied by courtesy of D. E. Chandler, Arizona State University, Tempe, Arizona.

of many simultaneous dimples in pancreatic acinar cells after exposing them to a secretagogue. The paper contains references to analogous demonstrations revealing the presence of pits and depressions also in pituitary and chromaffin cells prior to secretion.

Not surprisingly, the secretory granules have never been seen to form dimples on their own membrane, in accordance with the common perception that the plasma

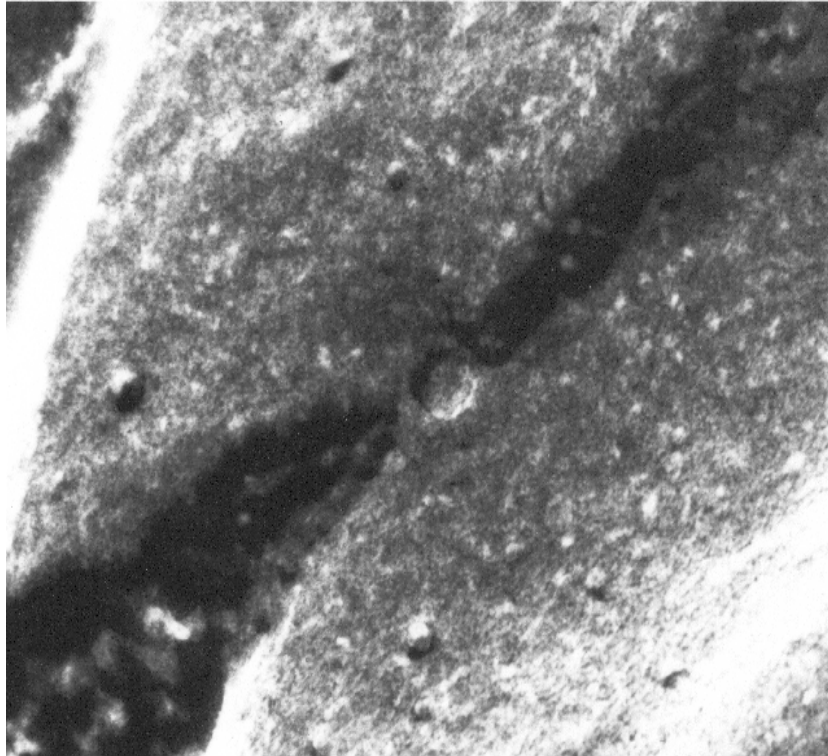


Fig. 5 The fusion pore shown as imprint of the plasma membrane dimple onto the granule membrane, from [37, Fig. 9C]. Reprinted with permission by Springer-Verlag. The high resolution micrograph was supplied by courtesy of D. E. Chandler, Arizona State University, Tempe, Arizona.

membranes are relatively slack and the membranes of densely packed granule under tension. That corresponds to our preceding Working Hypothesis No. 2.

2.6 The Flickering of Regulated Exocytosis

Another feature of the fusion pore making requires explanation (and is nicely explained by instabilities of the discussed AC current), namely the flickering of the fusion event, i.e., the common observation that the fusion pore can be maintained only after a while of opening and is not stable immediately after its making. Irregular rapid pore openings and closures are observed that last from a few milliseconds to many seconds, see Fernandez et al. [39] for fusion-pore flickering (*kiss-and-run*) in mast cells, and Rosenheck [23] and Jahn et al. [27] for wider reports on the observed flickering of the fusion event, mostly for synaptic vesicle exocytosis.

3 The Model

In this section we fix our notation and introduce the basic equations for the propagation of the electromagnetic (wandering) field wave and the making of the dimple.

3.1 The Force Balance Equation

Let $\mathbf{r} = \mathbf{r}(x, y, z, t)$ denote the displacement vector of the dimple and m the mass of an elementary unit of the dimple. Then the resulting force for making the dimple is approximately equal to $m \frac{\partial^2 \mathbf{r}}{\partial t^2}$, i.e. we can write

$$m \frac{\partial^2 \mathbf{r}}{\partial t^2} = \mathbf{F}_{elas} + \mathbf{F}_{vis} + \mathbf{F}_{ext}, \quad (3)$$

where \mathbf{F}_{elas} denotes the restoring (or elastic) force, \mathbf{F}_{vis} stands for viscosity reaction of the medium surrounded our plasme membrane, and \mathbf{F}_{ext} is an external force providing the membrane displacement from equilibrium state.

Our first task is to describe the restoring force \mathbf{F}_{elas} . In first approximation, we shall assume that the plasma membrane is a surface in \mathbb{R}^3 without bending resistance. Hence \mathbf{F}_{elas} is defined only by the surface tension and the variation of the membrane surface area.

To describe \mathbf{F}_{elas} and \mathbf{F}_{vis} more precisely, we adapt the standard text book model for the suspended vibrating string, respectively, vibrating plate (see, e.g., Churchill [40, Sect. 93] and Logan [41]). We consider $1D$ - and $2D$ -membranes separately, because the restoring force behaves differently in one-dimensional and many-dimensional cases. We begin with the $1D$ -case, since all the arguments are simpler in that situation.

3.2 The 1D-Case

In the equilibrium state, let our $1D$ -membrane coincide with the x -axis; let $u = u(x, t)$ denote the displacement of our plasma membrane from equilibrium state at the point x and at the time t ; and let $\rho = \rho(x)$ denote the linear membrane density at the point x . We restrict ourselves to sufficiently small deformations, so, for now, we will neglect all the terms that are of higher infinitesimal order with respect to $\frac{\partial u}{\partial t}$.

Since our plasma membrane has no bending resistance, its tension $\mathbf{T}(x, t)$ at the point x and at the time t is directed along the tangent to the membrane at x . Therefore, the unit $(x, x + \Delta x)$ is subjected to tensions $\mathbf{T}(x + \Delta x, t)$ and $-\mathbf{T}(x, t)$ (see Fig.

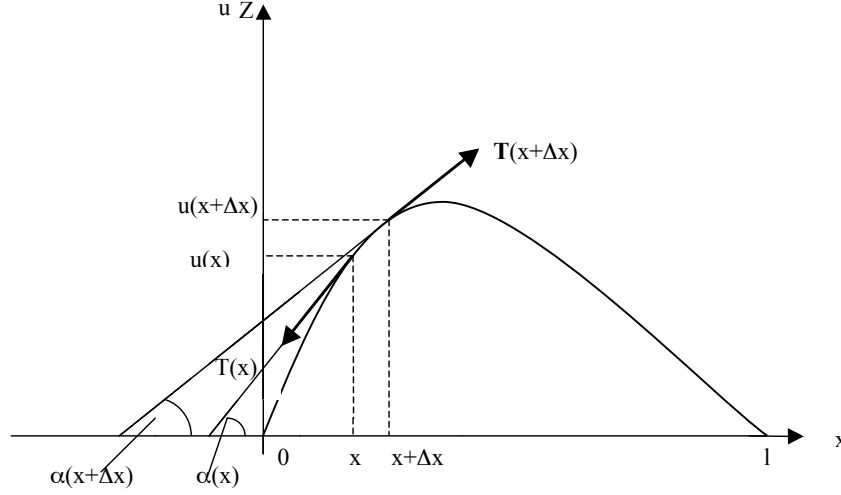


Fig. 6 Tension along the plasma membrane

6). Moreover, according to Hooke's law, $|\mathbf{T}(x, t)|$ does not depend on x and t , i.e., $|\mathbf{T}(x, t)| = \mathbf{T}_0$.

Defining T_1 as a relaxation time due to the action of the surrounded medium, we note that \mathbf{F}_{vis} is directed parallel to the vertical coordinate axis and can be modelled as being proportional to $\frac{1}{T_1} \frac{\partial u}{\partial t}$.

Let us denote by $f(x, t)$ the density of an external force \mathbf{F}_{ext} acting on the membrane point x at the time t and directing along the vertical axis. For a description of our electromagnetic candidate, see below Sect. 3.5.

Thus, projecting Eq. (3) onto the vertical coordinate axis and taking the preceding relations into account, we get the equality

$$\begin{aligned} & \rho \Delta x \frac{\partial^2 u}{\partial t^2} \\ &= T(x + \Delta x, t) \sin(\alpha(x + \Delta x)) - T(x, t) \sin \alpha(x) - \frac{2\rho}{T_1} \Delta x \frac{\partial u}{\partial t} + f(x, t) \Delta x. \end{aligned} \quad (4)$$

In the context of our approximation

$$\sin(\alpha) = \frac{\tan(\alpha)}{\sqrt{1 + \tan^2(\alpha)}} \approx \tan(\alpha) = \frac{\partial u}{\partial x},$$

and, consequently, equality (4) takes the form

$$\frac{\partial^2 u}{\partial t^2} = \frac{\mathbf{T}_0}{\rho \Delta x} \left[\frac{\partial u(x + \Delta x, t)}{\partial x} - \frac{\partial u(x, t)}{\partial x} \right] - \frac{2}{T_1} \frac{\partial u}{\partial t} + \frac{1}{\rho} f(x, t). \quad (5)$$

Passing in (5) to the limit as $\Delta x \rightarrow 0$ we arrive at

$$\frac{\partial^2 u}{\partial t^2} + \frac{2}{T_1} \frac{\partial u}{\partial t} - c_s^2 \frac{\partial^2 u}{\partial x^2} = \frac{1}{\rho} f(x,t), \quad (6)$$

where $c_s^2 = \frac{T_0}{\rho}$ is the speed of sound in the membrane.

3.3 The 2D-Case

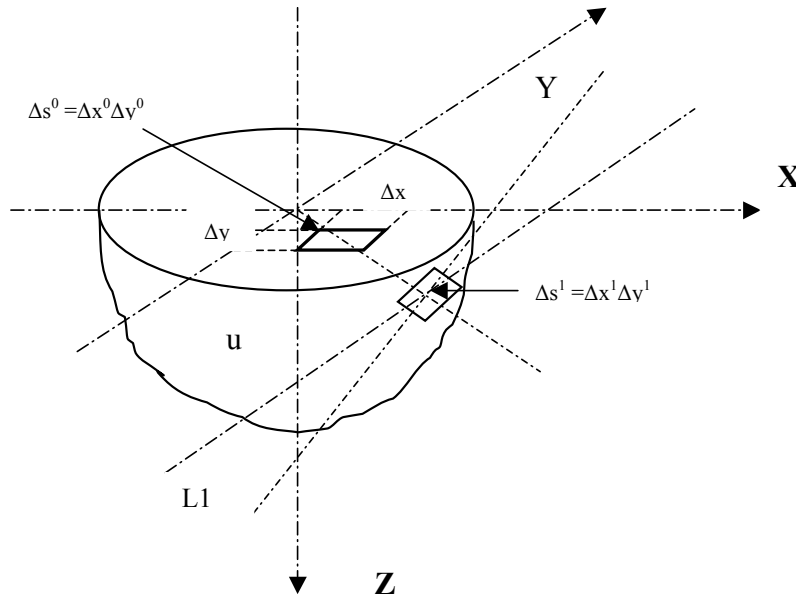


Fig. 7 Membrane displacement from equilibrium state at the point (x,y) and at the time t , notations

Similarly to the 1D-case we assume that in equilibrium state our plasma membrane lies in a subspace XY (see Fig. 7) and $u = u(x,y,t)$ denotes the membrane displacement from equilibrium state at the point (x,y) and at the time t . We will consider only small deformations such that

$$\left(\frac{\partial u}{\partial x}\right)^2 \ll 1, \quad \left(\frac{\partial u}{\partial y}\right)^2 \ll 1. \quad (7)$$

Let $d\sigma$ be the unit length of some closed path lying on the membrane surface, and let P be a point belonging to $d\sigma$. Then the unit $d\sigma$ is subjected to the tension

force $\mathbf{T}d\sigma$, where $\mathbf{T} = \mathbf{T}(x, y, t)$ denotes the surface tension. Due to absence of the membrane resistance to bending and shear, we can say that the vector \mathbf{T} always lies on the hyperplane L_1 tangential to the membrane surface at the point P , and \mathbf{T} is orthogonal to $d\sigma$ (see Fig. 7).

In addition, inequalities (7) guarantee that the tangential hyperplane L_1 lies almost parallel to the hyperplane XY . To prove this statement, we have to show that the length of the projection of the vector $\mathbf{T}(x, y, t)$ onto XY is approximately equal to $|\mathbf{T}(x, y, t)|$. Indeed, by definition

$$|\text{Projection}_{XY}\mathbf{T}(x, y, t)| = |\mathbf{T}(x, y, t)| \cos(\beta),$$

where β stands for the angle between the tension vector \mathbf{T} and hyperplane XY . It is easy to see that β is not bigger than the angle γ between the tangent hyperplane L_1 and XY . Therefore,

$$\cos(\beta) \geq \cos(\gamma) = \left[1 + \left(\frac{\partial u}{\partial x} \right)^2 + \left(\frac{\partial u}{\partial y} \right)^2 \right]^{-1/2} \approx 1,$$

and, consequently,

$$|\text{Projection}_{XY}\mathbf{T}(x, y, t)| \approx |\mathbf{T}(x, y, t)|.$$

Hooke's law guarantees that $|\mathbf{T}(x, y, t)|$ does not depend on the t -variable, whereas the orthogonality of $\mathbf{T}(x, y, t)$ and $d\sigma$ provides the independence of $|\mathbf{T}|$ on the variables x and y as well. It means that

$$|\mathbf{T}(x, y, t)| = \mathbf{T}_0 = \text{const.}$$

Now, considering a rectangle unit $ds = \Delta x \Delta y$ on the membrane surface, we can write the restoring force acting on this unit as:

$$\begin{aligned} \mathbf{T}_0 \Delta y \left[\left(\frac{\partial u}{\partial x} \right) \Big|_{x+\frac{\Delta x}{2}} - \left(\frac{\partial u}{\partial x} \right) \Big|_{x-\frac{\Delta x}{2}} \right] + \mathbf{T}_0 \Delta x \left[\left(\frac{\partial u}{\partial y} \right) \Big|_{y+\frac{\Delta y}{2}} - \left(\frac{\partial u}{\partial y} \right) \Big|_{y-\frac{\Delta y}{2}} \right] \\ = \mathbf{T}_0 \Delta y \frac{\partial^2 u}{\partial x^2} \Delta x + \mathbf{T}_0 \Delta x \frac{\partial^2 u}{\partial y^2} \Delta y = \mathbf{T}_0 \left(\frac{\partial^2 u}{\partial x^2} + \frac{\partial^2 u}{\partial y^2} \right) \Delta x \Delta y. \end{aligned}$$

It remains to describe the external and viscosity forces acting on ds . Similarly to the $1D$ -case, $f(x, y, t)$ denotes the density of the external force \mathbf{F}_{ext} at the point x and at the time t . It is directed orthogonally to the membrane surface, while \mathbf{F}_{vis} , directed opposite to the vector \mathbf{F}_{ext} , is proportional to the velocity $\frac{\partial u}{\partial t}$.

Let $\rho(x, y)$ denote the membrane surface density, then the mass of the unit ds is equal $\rho(x, y) \Delta x \Delta y$. Finally, defining a relaxation time due to the action of the surrounded medium by T_1 , we can write the variant of Eq. (3) for $2D$ -membranes as follows:

$$\rho \Delta x \Delta y \frac{\partial^2 u}{\partial t^2} = \mathbf{T}_0 \left(\frac{\partial^2 u}{\partial x^2} + \frac{\partial^2 u}{\partial y^2} \right) - \frac{2\rho}{T_1} \Delta x \Delta y \frac{\partial u}{\partial t} + f(x, y, t) \Delta x \Delta y. \quad (8)$$

After elementary transformations, Eq. (8) takes the form

$$\frac{\partial^2 u}{\partial t^2} + \frac{2}{T_1} \frac{\partial u}{\partial t} - c_s^2 \left(\frac{\partial^2 u}{\partial x^2} + \frac{\partial^2 u}{\partial y^2} \right) = \frac{1}{\rho} f(x, y, t), \quad c_s^2 = \frac{\mathbf{T}_0}{\rho}. \quad (9)$$

3.4 Further Approximations

Having equations (6) and (9) at hands, we observe that the process of dimple forming is quasi-static, i.e.,

$$\frac{\partial^2 u}{\partial t^2} \ll 1.$$

The latter means that we can neglect this term in both equations.

It should be also pointed out that $u = |Du| = 0$ at those membrane points where there is no influence of the external force. Here Du denotes the spatial gradient of the displacement u .

Recall that the characteristic function χ_E of a set E is defined by

$$\chi_E(z) = \begin{cases} 1, & \text{for } z \in E, \\ 0, & \text{for } z \notin E. \end{cases}$$

Taking into account all the above remarks we get the following model equations for the dimple forming in the one- and two-dimensional cases, respectively:

$$\frac{2}{T_1} \frac{\partial u}{\partial t} - c_s^2 \frac{\partial^2 u}{\partial x^2} = \frac{1}{\rho} f(x, t) \chi_{\{u>0\}}, \quad (10)$$

$$\frac{2}{T_1} \frac{\partial u}{\partial t} - c_s^2 \left(\frac{\partial^2 u}{\partial x^2} + \frac{\partial^2 u}{\partial y^2} \right) = \frac{1}{\rho} f(x, y, t) \chi_{\{u>0\}}. \quad (11)$$

3.5 Lorentz Force

Clearly, there is a variety of external forces resulting from the electromagnetic field wave. One can expect that they all play together in forming the dimple. However, taking our point of departure in an alternating current, we shall concentrate on the *Lorentz force*, (implicitly deal with the *Coulomb force*), but discard the *dipole electric force*, the *magnetic force*, and the *van der Waals force* for now.

3.5.1 Pecularity of the Lorentz Force

In our physiological context, the peculiar role of the Lorentz force is, that it exerts its action in one fixed direction, the direction of the propagation of the field wave, even it is related to an alternating current. Roughly speaking, that's the sophistication and power of the electromagnetic aspects of the regulated exocytosis, that a relatively weak and extremely low frequent electrodynamic wave can transport energy along a straight line over a large intracellular distance and exert its action on the charged phospholipid molecules in the plasma membrane. These charged molecules make a substantial part of the eukaryotic plasma membrane, around 11% according to Rosenheck [23].

3.5.2 Energy Estimates

It may be instructive to have a rough idea of the scale of the electric forces and related energies around the dimple formation. Based on the estimates given by Rosenheck l.c., we have a surplus of about 10^{10} (negative) charges per 1000 nm^2 plasma membrane area, i.e., about 10^9 charge carriers around the dimple top stretching over an area of approximately 100 nm^2 . The energy of one charged phospholipid molecule was calculated by Rosenheck l.c. as being $10^{-19} \text{ W sec} = 10^{-19} \text{ Nm}$. Dividing by a characteristic length of 10 nm we obtain a force of around 10^{-11} N , i.e., a total force of 10^{-2} N exerted on the dimple region.

For comparison, the gravitational force of the mass 10^{-21} kg of a dimple of about 10^3 nm volume (and specific weight comparable to water) would only sum up to $10^{-21} \times 9.8 \sim 10^{-20} \text{ N}$. For another comparison, we refer to the Koch-Stetter electromagnetic field wave generator. For now, its B-field is of about 35 mT (milliTesla) and the exerted forces are visible and can be measured.

To sum up, for the making of the dimple we are investigating electric forces which surpass by large the above estimated 10^{-2} N .

3.5.3 Model Quantities

Our first model quantity is the capacitive reactance X_C as scalar function of place and time, depending on the shape of the dimple. Our second model quantity is the time dependent (namely dimple shape and X_C dependent) amplitude \vec{B} of the magnetic flux density.

3.5.4 Model Equations

As mentioned before, we have two model levels.

(I) There must be a variational equation, minimizing an energy functional or another related cost functional which gives the change and spatial distribution of X_C .

(II) As discussed above, there are also elastic and viscous forces resisting the necessary re-packing of the lipid heads under deformation and pulling the plasma membrane back in the more smooth non-dimple form, interrupting exocytosis when the electrical and magnetic production is interrupted.

3.5.5 The Lorentz force

Our favorite external force for making the dimple is the Lorentz force

$$\mathbf{F}_L = q\mathbf{E}_0 + q(\mathbf{v} \times \mathbf{B}) - \gamma\mathbf{v}, \quad (12)$$

where q is the charge (i.e., twice the number) of the released Ca^{2+} ions, \mathbf{E}_0 is the background electric field, here assumed to be zero, \mathbf{B} is the magnetic flux density, \mathbf{v} is the velocity of the charged dimple particles with respect to the coordinate system in which the quantities \mathbf{F} , \mathbf{E}_0 , and \mathbf{B} are calculated, i.e., \mathbf{v} is up to the sign the wandering velocity of the directed electromagnetic field wave, and $\gamma\mathbf{v}$ is the friction force under propagation. Once again, equation (12) is written in SI. In the cgs system, common in physics, the term $q(\mathbf{v} \times \mathbf{B})$ has to be divided by c , the velocity of light in vacuum.

Note that we have for a (moving) field wave (see, e.g., [42, Chapter 13])

$$\mathbf{B}(\mathbf{x}, t) = \widehat{\mathbf{B}} \cos(\mathbf{k} \cdot \mathbf{x}(t) - kv(\mathbf{x}, t)t) + \mathbf{B}_{\text{DC}}, \quad (13)$$

$$\mathbf{E}(\mathbf{x}, t) = \mathbf{v}(\mathbf{x}, t) \times \mathbf{B}(\mathbf{x}, t). \quad (14)$$

Here, \mathbf{B}_{DC} denotes the background B-field corresponding to the direct current \mathbf{E}_0 , $\mathbf{x} = (x, y, z)$ denotes a position, \mathbf{k} denotes the wave vector with $k = |\mathbf{k}|$ and $v(\mathbf{x}, t) = |\mathbf{v}(\mathbf{x}, t)|$.

The Lorentz force of Eq. (12) can be inserted into the general balance equation (3), into the 1-dimensional model equations (4), (6), simplified to (10), and into the 2-dimensional model equations (8), simplified to (11).

3.5.6 Work Equation

In Sect. 2.4, we have sketched the feedback mechanism of the dimple forming and explained why and how the forming of the dimple strengthens the electromagnetic field wave. It is beyond the range of this chapter to model that mechanism in detail as a free boundary problem. Basically, to relate our defining quantity X_C to the listed balance equations, we shall express the power in terms of X_C and then derive an integral for the electromagnetic energy density (per volume), where X_C enters. The details will be worked out separately.

4 Apposite Results on Parabolic Obstacle Problems

At the end of Sect. 3.4, we introduced the model equations (10) and (11) that can be treated as parabolic free boundary problems (FBP).

4.1 Review of Free Boundary Problems

The expression **free boundary problem** means that we deal with a problem with two a-priori unknown objects: an unknown *set* coming up in a *solution* of a partial differential equation.

A typical example is the *Stefan problem* describing the melting of an ice cube in a glass of water. If ice begins to melt then the region occupied by water will grow and the interface-surface between the ice and the water (it is called the free boundary) will move and change its shape, see, e.g., Friedman [43, Sect. 1.9]. As another typical example of FBP we mention the flame propagation problem describing the evolution of the flame front, for that see the various contributions in [44, Chapter 8].

Using a common transformation of the independent variables, we may normalize the coefficients and so reduce our model equations (10) and (11) to the following problem:

$$\begin{cases} \Delta u(x,t) - \frac{\partial u}{\partial t}(x,t) = f(x,t)\chi_{\{u>0\}}, & \text{almost everywhere (a.e.) in } \mathcal{D}, \\ u(x,t) \geq 0 \end{cases} \quad (15)$$

where (x,t) denotes the points in $\mathbb{R}^n \times \mathbb{R}$ with the space variable $x = (x_1, \dots, x_n)$ belonging to \mathbb{R}^n and the time variable t belonging to \mathbb{R} , Δ is the Laplace operator defined as

$$\Delta u = \sum_{i=1}^n \frac{\partial^2 u}{\partial x_i^2},$$

$\chi_{\{u>0\}}$ is the characteristic function of the set $\{(x,t) \in \mathbb{R}^{n+1} \mid u > 0\}$ (see Section 3.4 for the precise definition), \mathcal{D} is a given open set in \mathbb{R}^{n+1} and u is a locally bounded weak (i.e., in the distributional sense) solution.

Observe that $\{u > 0\}$ is a priori an unknown open subset of \mathcal{D} . We denote by Γ the intersection of \mathcal{D} with the *boundary* of the set $\{u = 0\}$. We will call Γ the *free boundary*. For our dimple forming, we have $\Gamma = \{\Gamma(t), \{t\}\}_{t \geq 0}$ of Fig. 3.

If, additionally, the condition

$$\frac{\partial u}{\partial t} \geq 0 \quad \text{a.e. in } \mathcal{D}, \quad (16)$$

is satisfied, then our FBP (15) becomes the Stefan problem mentioned above. Inequality (16) means that our dimple is formed without “returning back”. In general,

however, we can not guarantee (16) from the assumptions given in Sections 3.2 and 3.3 only.

For the function $f(x, t)$, we assume that

- (1) f is *non-degenerate* in \mathcal{D} , i.e., there exists $\delta_0 > 0$ such that $f(x, t) > \delta_0$ for any $(x, t) \in \mathcal{D}$;
- (2) f is *Hölder continuous* in \mathcal{D} with some $\alpha \in (0, 1)$, i.e., f is a bounded continuous function in \mathcal{D} , and for all points (x, t) and $(y, s) \in \mathcal{D}$ such that $(x, t) \neq (y, s)$ we have the inequality

$$\frac{|f(x, t) - f(y, s)|}{(|x - y|^2 + |t - s|^2)^{\alpha/2}} < \infty.$$

4.2 Qualitative Properties of Solutions

Let u be a solution of FBP (15), let $z^0 = (x^0, t^0) \in \mathcal{D}$, let $\rho > 0$ sufficiently small, and let $Q_\rho(z^0) := \{|x - x^0| < \rho\} \times (t^0 - \rho^2, t^0)$. The following estimates provide us with information about the behaviour of our displacement u near the interface between the sets $\{u > 0\}$ and $\{u = 0\}$, i.e., near the free boundary.

- There exists a constant $c = c(n) > 0$ such that

$$\sup_{Q_\rho(z^0)} u \geq c(n)\rho^2. \quad (17)$$

This nondegeneracy estimate holds true for all points z^0 belonging to the closure of the set $\{u > 0\}$ and for all ρ sufficiently small.

Moreover, our solution u has quadratic growth near the free boundary:

- There exists a constant $C > 0$ such that

$$\sup_{Q_\rho(z^0)} u \leq C\rho^2. \quad (18)$$

This nondegeneracy estimate holds true for all free boundary points $z^0 \in \Gamma$ and for all ρ sufficiently small.

- There exists a universal constant $M > 0$ such that

$$\sup_{Q_\rho(z^0) \cap \{u > 0\}} \left(\left| \frac{\partial^2 u}{\partial x_i \partial x_j} \right| + \left| \frac{\partial u}{\partial t} \right| \right) \leq M. \quad (19)$$

This inequality holds true for all free boundary points $z^0 \in \Gamma$ and for all ρ sufficiently small.

For $f(x, t) = \text{const}$ all these three statements were proved in [45]. The case of general $f = f(x, t)$ was considered in [46] for $n > 1$ and in [47] for $n = 1$.

The preceding estimates (17), (18), and (19) indicate that characteristic base diameter, growth rate, depth and time of the dimple forming are mathematically well defined and, therefore, these values should, in principle, be measurable in experiment, see below Sect. 5.2.

4.3 Classification of Blow-up Limits in \mathbb{R}^{n+1}

The idea is to use *blow-up* sequences, which are kind of zooms, and to look at the "infinite zoom". Suppose that u is a solution of the problem (15), $z^* = (x^*, t^*)$ is a free boundary point and $f(x^*, t^*) \neq 0$. For $\lambda > 0$ consider the functions

$$u_\lambda(x, t) := \frac{u\left(x^* + x \frac{\lambda}{\sqrt{f(x^*, t^*)}}, t^* + t \frac{\lambda^2}{f(x^*, t^*)}\right)}{\lambda^2}, \quad \text{for } (x, t) \in \mathcal{D}_\lambda := \frac{1}{\lambda} \mathcal{D}.$$

There exists a sub-sequence $\{\lambda_k\}$ converging to zero such that the blow-up sequence $\{u_{\lambda_k}\}$ converges to one of the following blow-up limits:

- $u_0 = u_{0,e}(x, t) := \frac{1}{2}(x^T \cdot \mathbf{e})^2$, for a unit vector \mathbf{e} , where $x^T \cdot \mathbf{e}$ denotes the scalar product in \mathbb{R}^n ,
- $u_0 = u_{0,m}(x, t) = mt + x^T \cdot \mathcal{M} \cdot x$, where m is a constant and \mathcal{M} is a $(n \times n)$ -matrix satisfying $\text{Tr} \mathcal{M} = m + 1$.

Observe that the blow-up limits can (in general) depend on the choice of the sub-sequence $\{\lambda_k\}$. But it should be emphasized that in view of the non-negativity of u the limit function u_0 is the unique non-negative distributional solution of

$$\Delta u - \frac{\partial u}{\partial t} = \chi_{u>0} \quad \text{a.e. in } \mathbb{R}^n \times (-\infty, t^*).$$

This means that in the second case m and \mathcal{M} are defined uniquely as well.

For $f(x, t) = \text{const}$ these results were obtained in [45]. For the general case $f = f(x, t)$ we refer the reader to [46].

4.4 Classification of the Free Boundary Points

Going to the regularity properties of the free boundary we observe firstly that

- The free boundary is a closed set of zero $(n + 1)$ -Lebesgue measure.
- The free boundary $\Gamma = \{\text{"regular points"}\} \cup \{\text{"singular points"}\}$.

- The set of the singular free boundary points is closed.

The *singular points* are defined as the free boundary points for those there exists a blow-up limit of the second type, i.e., $u^0(x, t) = mt + x^T \cdot \mathcal{M} \cdot x$. The set $\Gamma \setminus \{\text{''singular points''}\}$ is the set of regular points. In addition for singular points and for $k = 0, \dots, n$ the sets $S(k)$ are considered, where $S(k)$ is defined as the set of singular points such that $\dim \text{Kern } \mathcal{M} = k$ and the smallest of the k non-zero eigenvalues is bounded from below by a fixed positive constant.

The complete classification of all free boundary points can be given via a relatively new approach introduced by G.S. Weiss in [48]. For a solution u of FBP (15) and for a free boundary point $z^* = (x^*, t^*)$ consider the following energy functional

$$W(\tau, z^*, u, f) := \frac{1}{\tau^4} \int_{t^* - 4\tau^2}^{t^* - \tau^2} \int_{|x - x^*| < \tau} \left(|\nabla u|^2 + 2fu + \frac{u^2}{t - t^*} \right) G(x - x^*, t^* - t) dx dt,$$

where $G(x, t)$ is the heat kernel.

The functional W has the following remarkable properties:

- $\lim_{\tau \rightarrow 0^+} W(\tau, z^*, u, f)$ exists and is finite;
- There are only two possible values for $\lim_{\tau \rightarrow 0^+} W(\tau, z^*, u, f)$, namely

$$\lim_{\tau \rightarrow 0^+} W(\tau, z^*, u, f) = \begin{cases} A_n, & \text{if } z^* \text{ is a regular point} \\ 2A_n, & \text{if } z^* \text{ is a singular point} \end{cases}$$

for some constant $A_n > 0$ depending only on the dimension n .

Finally, we observe that

- Around regular points the free boundary is a smooth graph.
- Singular points belonging to $S(n)$ are isolated.
- $S(n)$ is contained locally in a C_x^2 -graph in space.
- $S(k)$ for $0 \leq k \leq n - 1$ is contained locally in a k -manifold of class $C_{x,t}^{1/2}$.

For all results concerning the regular points we refer to [45]. The results about singular points were proved in [46] (see also [49]).

5 Conclusions

Our conclusions consist of preliminary findings which will require further experiments and measurements to be confirmed - or falsified.

5.1 *The Findings*

We have provided a mathematical model for the initiation of regulated exocytosis and the making of the fusion pore. The model relates the geometry and the dynamics of one single membrane process, namely the forming of an inward oriented dimple in the plasma membrane before the fusion event, with electromagnetic features of intracellular calcium oscillations. The model suggests a new explanation for the observed flickering of regulated exocytosis, the vanishing of the first phase of secretion in stressed or tired β -cells and the final halt of all secretion in overworked afunctional cells: the electromagnetic free boundary model points to the lack of stability and coordination of the intracellular Ca^{2+} oscillations prior to the bilayer membrane vesicle fusion. We recall that the field character of these oscillations is magnetic (therefore transferring energy to the fusion site at the plasma membrane without any loss). It must be distinguished from the widely studied Ca^{2+} influx changing the electrostatic potential across the plasma membrane and accompanying regulated exocytosis.

The model is based solely on physical First Principles. All parameters have a biophysical meaning and can, in principle, be measured.

5.2 *Suggested Experiments and Measurements*

At the present stage of our knowledge, the mathematical and biophysical *correctness* of our model doesn't prove its *relevance* for explaining the phenomena it claims to explain. To decide whether the here described phenomena and effects are *dispensable* or *decisive* for regulated exocytosis, the scales of the ion oscillations, the electromagnetic fields, the acting forces, the entering material constants and the characteristic times and lengths must be determined.

Hence, the framework of our electromagnetic free boundary problem for the dimple making suggest the following array of experiments and measurements:

1. We shall observe the Ca^{2+} oscillations prior to the bilayer membrane vesicle fusion also in pancreatic β -cells and determine their spatial and temporal character. In particular, the observations must
 - check the intracellular origin of the oscillations; we may, e.g., deliberately silence (empty) some types of organelles by adding suitable agents, see, e.g., Fridlyand et al. [50];
 - identify the participating organelles (Ca^{2+} storages); and
 - decide about the orientation (the direction) of oscillations, the frequency, depending on stimulus, and the distinction between almost simultaneous oscillations pointing in different directions as their selected sites for the making of the fusion pore.

2. We shall modulate the oscillations by submitting the cells to an external field generator with variable frequencies, to prove the magnetic character of the field wave associated to the oscillations.
3. We shall determine the surface tension in the plasma membrane of living cells. In particular, we shall measure and/or calculate the bending rigidity and stretching elasticity under "repacking" of the ball shaped heads of the inner lipids under area changes. For living cells, we expect that these magnitudes are substantially larger than for model membranes, e.g., due to osmotic pressure in living cells, see Henriksen and Ipsen [51].
4. We shall measure the cytosol viscosity close to the plasma membrane, i.e., update the classic study [52] by Bicknese et al., and locate actin filaments blocking for unwanted docking of the insulin granules at the plasma membrane.
5. We shall check Rosenheck's estimate (l.c.) for charged molecules in the plasma membrane.
6. We shall estimate the content of magnetizable Fe atoms in the membranes.
7. We need precise electron or atomic force microscope slices of the dimple making and of the degree of its singularity in β -cells.
8. We shall measure by patch clamp technique the expected decrease of the capacitive reactance X_C under dimple forming.
9. We shall correlate the Ca^{2+} oscillations with the fusion events; in particular, we shall confirm the spatial and temporal coincidence of flickering of exocytosis with break-downs of the field wave.
10. We shall demonstrate the absence or weakness of the Ca^{2+} oscillations after stimulation in stressed or tired β -cells.

Acknowledgements The first author was partially supported by the Russian Foundation for Basic Research (grant no. 09-01-00729). The third author acknowledges the support by the Danish network *Modeling, Estimation and Control of Biotechnological Systems (MECOBS)*.

References

1. B. Alberts et al., *Molecular Biology of the Cell*, 4th edn. (Garland Science, Taylor and Francis Group, New York, 2002), p. 757.
2. M. Koch et al., Can single electrons initiate fusion of biological membranes? *Biophys. Rev. Lett.* **2/1**, 23–31 (January 2007).
3. B. R. Lentz et al., Protein machines and lipid assemblies: current views of cell membrane fusion, *Curr. Opin. Struct. Biol.* **10**, 607–615 (2000).
4. P. Rorsman and E. Renström, Insulin granule dynamics in pancreatic beta cells, *Diabetologia* **46**, 1029–1045 (2003).
5. E. Renström and P. Rorsman, Regulation of insulin granule exocytosis, in: S. Seino, G.I. Bell (eds.), *Pancreatic Beta Cell in Health and Disease*, Springer-Verlag Tokyo, 2007, pp. 146–176.
6. P. de Meyts, Connecting the dots in the pathogenesis of type-2 diabetes: the need for systems biology, this volume.
7. J. C. Shillcock and R. Lipowsky, The computational route from bilayer membranes to vesicle fusion, *J. Phys.: Condens. Matter* **18**, S1191–S1219 (2006).

8. G. M. Grodsky, A threshold distribution hypothesis for packet storage of insulin and its mathematical modelling, *J. Clin. Invest.* **51**, 2047–2059 (Aug 1972). 1972.
9. Chen, Wang and Sherman, Identifying the targets of the amplifying pathway for insulin secretion in pancreatic beta cells by kinetic modeling of granule exocytosis, *Biophys. J.* **95/5**, 2226–2241 (Sept. 2008).
10. J. K. Larsen and M. G. Pedersen, Compartment models for regulated exocytosis, in [11].
11. B. Booß-Bavnbek et al. (eds.), *BetaSys - Systems Biology of Regulated Exocytosis in Pancreatic β -Cells*, Springer-Verlag, New York, Series *Systems Biology* vol. 4, to appear.
12. J. Shillcock, Probing cellular dynamics with mesoscopic simulations, [11].
13. R. E. Caflisch and B. Li, Analysis of island dynamics in epitaxial growth of thin films, *Multi-scale Model. Sim.* **1/1**, 150–171 (2002).
14. C. Le Bris, Mathematical and numerical analysis for molecular simulation: accomplishments and challenges, in *Proc. Int. Cong. Mathematicians, Madrid 2006*, eds. M. Sanz-Solé et al. (European Mathematical Society, Zürich, 2006), p. 1506.
15. B. V. Bazalyi and A. Friedman, A free boundary problem for an elliptic-parabolic system: application to a model of tumor growth, *Comm. Partial Differential Equations* **28/3-4**, 517–560 (2003).
16. B. Bazalyi and A. Friedman, Global existence and asymptotic stability for an elliptic-parabolic free boundary problem: an application to a model of tumor growth, *Indiana Univ. Math. J.* **52/5**, 1265–1304 (2003).
17. Y. Tao, N. Yoshida and Q. Guo, Nonlinear analysis of a model of vascular tumor growth and treatment, *Nonlinearity* **17**, 867–895 (2004).
18. Y. Tao and M. Chen, An elliptichyperbolic free boundary problem modelling cancer therapy, *Nonlinearity* **19**, 419–440 (2006).
19. D. Ni, H. Shi and Y. Yin, Theoretical analysis of adhering lipid vesicles with free edges, *Colloids and Surfaces B: Biointerfaces* **46**, 162–168 (2005).
20. L. E. Fridlyand and L. H. Philipson, Metabolic oscillations in β -cells, [11].
21. J. D. Jackson, *Classical Electrodynamics*, 3rd ed., John Wiley, New York, 1999.
22. J. R. Monck and J. M. Fernandez, The exocytotic fusion pore, *J. Cell. Biol.* **119/6**, 1395–1404 (Dec. 1992).
23. K. Rosenheck, Evaluation of the electrostatic field strength at the site of exocytosis in adrenal chromaffin cells, *Biophys. J.* **75**, 1237–1243 (Sept. 1998).
24. M. Kraus, B. Wolf and Be. Wolf, Crosstalk between cellular morphology and calcium oscillation patterns Insights from a stochastic computer model, *Cell Calcium* **19/6**, 461–472 (June 1996).
25. Be. Wolf, <http://www.lme.ei.tum.de/englisch/research/microscopy.htm>.
26. C. Salazar, A. Z. Politi, and T. Höfer, Decoding of calcium oscillations by phosphorylation cycles: analytic results, *Biophysical Journal* **94**, 1203–1215 (February 2008).
27. R. Jahn, T. Lang, and T. C. Südhoff, Membrane fusion, *Cell* **112**, 519–533 (February 21, 2003).
28. M. J. Berridge, M. D. Bootman, and H. L. Roderick, Ca^{2+} signaling: dynamics, homeostasis and remodeling, *Nat. Rev. Mol. Cell Biol.* **4**, 517–529 (2003).
29. L. D. Gaspers and A. P. Thomas, Calcium signaling in liver, *Cell Calcium* **38**, 329–342 (2005).
30. A. B. Noske, A. J. Costin, G. P. Morgan, and B. J. Marsh, Expedited approaches to whole cell electron tomography and organelle mark-up in situ in high-pressure frozen pancreatic islets, *J. Struct. Biol.* **161/3**, 298–313 (2007).
31. A. B. Noske and B. J. Marsh, Mapping the β -cell in 3D at the nanoscale using novel cellular electron tomography and computational approaches, in [11].
32. M. Koch, <http://www.feldkraft.de/>.
33. K. A. Jensen, *Almen Kemi*, Copenhagen, 1957.
34. R. B. Frankel and R. P. Blakemore (eds.), *Iron Biominerals - Proceedings of a Conference on Iron Biominerals, held July 31–August 1, 1989, at the University of New Hampshire, Durham*, Plenum Press, New York, 1991.
35. D. E. Chandler and J. Heuser, Membrane fusion during secretion, *J. Cell Biology* **83**, 91–108 (October 1979).

36. D. E. Chandler and J. Heuser, Arrest of membrane fusion events in mast cells by quick-freezing, *J. Cell Biology* **86/2**, 666–674 (Aug. 1980).
37. M. J. Curran, F. S. Cohen, D. E. Chandler, P. J. Munson, and J. Zimmerberg, Exocytotic fusion pores exhibit semi-stable states, *J. Membrane Biol.* **133**, 61–75 (October 1993).
38. B. P. Jena, S.-J. Cho, A. Jeremic, M. H. Stromer, and R. Abu-Hamdah, Structure and composition of the fusion pore, *Biophys. J.* **84**, 1337–1343 (February 2003).
39. J. M. Fernandez, E. Neher, and B. D. Gomperts, Capacitance measurements reveal stepwise fusion events in degranulating mast cells, *Nature* **312**, 453–455 (1984).
40. R. V. Churchill, *Operational Mathematics*, 3rd ed., Mc Graw Hill, Boston, 1958.
41. J. D. Logan, *Applied Partial Differential Equations*, 2. ed., Undergraduate Texts in Mathematics, Springer, 2004.
42. P. A. Tipler, *Physics for Scientists and Engineers*, 3. ed., New York, NY: Worth Publishers, 1991.
43. A. Friedman, *Variational Principles and Free-boundary Problems*, Wiley (Pure and applied mathematics), 1982.
44. A. Fasano and M. Primicerio (eds.), *Free Boundary Problems: Theory and Applications*, vol. 2, Pitman Books Ltd., London, 1983.
45. L. A. Caffarelli, A. Petrosyan and H. Shahgholian, Regularity of a free boundary in parabolic potential theory, *J. Amer. Math. Soc.* **17**, 827–869 (electronic) (2004).
46. A. Blanchet, On the singular set of the parabolic obstacle problem, *J. Differential Equations* **231**, 656–672 (2006).
47. A. Blanchet, J. Dolbeault, and R. Monneau, *Erratum of "On the continuity of the time derivative of the solution to the parabolic obstacle problem with variable coefficients*, preprint (2005).
48. G. S. Weiss, Self-similar blow-up and Hausdorff dimension estimates for a class of parabolic free boundary problems, *SIAM J. Math. Anal.* **30**, 623–644 (electronic) (1999).
49. A. Blanchet, On the regularity of the free boundary in the parabolic obstacle problem. Application to American options, *Nonlinear Analysis* **65**, 1362–1378 (2006).
50. L. E. Fridlyand, N. Tamarina, and L. H. Philipson, Modeling the Ca^{2+} flux in pancreatic beta-cells: role of the plasma membrane and intracellular stores, *Am. J. Physiol. Endocrinol. Metab.* **285**, E138-E154 (2003).
51. J. R. Henriksen and J. H. Ipsen, Measurement of membrane elasticity by micro-pipette aspiration, *Eur. Phys. J. E* **14**, 149–167 (2004).
52. S. Bicknese, N. Periasamy, S. B. Shohet, and A. S. Verkman, Cytoplasmic viscosity near the cell plasma membrane: measurement by evanescent field frequency-domain microfluorimetry. *Biophys. J.* **65**, 1272-1282 (September 1993).